Polymer Journal (2016) 48, 801–806

www.nature.com/pj

ORIGINAL ARTICLE

Anomalous small-angle X-ray scattering study on the spatial distribution of hydrophobic molecules in polymer micelles

Ryosuke Nakanishi, Ginpei Machida, Masaki Kinoshita, Kazuo Sakurai and Isamu Akiba

The spatial distribution of bromine-labeled hydrophobic molecules—bromobenzene (BrBz) and 4-bromobenzylalcohol (BrBzOH)—incorporated in polymer micelles of poly(*N*,*N*-dimethylaminoethyl methacrylate)-*block*-poly(methyl methacrylate) (PDMAEMA-*b*-PMMA) was investigated using anomalous small-angle X-ray scattering (ASAXS) near the Br K-edge. Both BrBz and BrBzOH were miscible with PMMA at all concentrations. ASAXS analyses revealed that BrBzOH was homogeneously dispersed in the hydrophobic PMMA core of the PDMAEMA-*b*-PMMA micelle, whereas BrBz was excluded from the vicinity of the core–shell interface of the PMMA core. Because of its hydrophobicity, BrBz resisted contact with water penetrating the PMMA core. Inevitably, a BrBz depletion layer formed in the vicinity of the core–shell interface. Conversely, because BrBzOH has an affinity for water due to its hydroxyl group, it can exist even in the vicinity of the core–shell interface of the PMMA core. The results of the present study suggest that the spatial distribution of hydrophobic molecules in polymer micelles can be controlled by tuning the polarity of the encapsulated species.
Polymer Journal (2016) **48,** 801–806; doi:10.1038/pj.2016.32; published online 16 March 2016

INTRODUCTION

When amphiphilic block copolymers are dissolved in water, they undergo self-assembly into polymer micelles consisting of a hydrophobic core and a hydrated corona.[1] Because polymer micelles can accept hydrophobic molecules into their hydrophobic core,[2,3] prolonging the blood circulation of the encapsulated species,[2–4] and their size allows them to accumulate around a tumor,[5–8] they have attracted attention as drug carriers in drug delivery systems.

Regarding the design of drug delivery system carriers, the stable retention and high concentration of drug molecules in polymer micelles are key characteristics.[9–11] The drug concentration of polymer micelles can be controlled by tuning the intermolecular interactions between drug molecules and the amphiphilic block copolymers of the micelle.[9–11] However, the retention of drug molecules in polymer micelles is difficult to control, and minor differences in the chemical structure of drug molecules cause significant changes in the release properties of drugs from polymer micelles.[11] For example, although polymer micelles composed of partially benzyl-substituted poly(ethylene glycol)-*block*-poly(aspartic acid) (PEG-P(Asp(Bzl))) can incorporate almost the same amount of synthetic retinoids Am80 and LE540, Am80 is rapidly released from PEG-P(Asp(Bzl)) micelles compared with the extremely stable retention of LE540.[11] When hydrophobic drug molecules are released from polymer micelles, they must pass through the hydrophobic core, core–corona interface and corona layer. Consequently, the retention or release rate of drug molecules depends not only on the interaction between drug molecules and block copolymers but also on the spatial distribution of drug molecules in the polymer micelle.[12] Therefore, the molecular origin of the spatial distribution of hydrophobic molecules in polymer micelles should be determined. Although the importance of spatial distribution and its mechanism of origin have been recognized, *in situ* techniques to determine how the drug molecules became dispersed in the polymer micelles have not yet been developed.

Anomalous small-angle X-ray scattering (ASAXS), which is the energy dependence of the intensity of X-ray scattering in small-angle regions measured at the energy of the incident X-ray near the absorption edge of a targeted element, is a powerful tool for analyzing the spatial distribution of a target element in nano-sized particles such as metal nanoparticles and polymer micelles.[13–25] Of the elements that can be analyzed by ASAXS, Br is suitable for polymer systems because it can be easily introduced into organic molecules.[22–25] Therefore, the ASAXS near the Br K-edge can be used to determine the spatial distribution of Br-labeled hydrophobic molecules in polymer micelles. In the present study, we applied ASAXS near the Br K-edge to the polymer micelles containing bromobenzene (BrBz) or 4-bromobenzylalcohol (BrBzOH) as Br-labeled hydrophobic molecules with the aim of elucidating the effects of the polarity and hydrophobicity

Department of Chemistry and Biochemistry, University of Kitakyushu, Kitakyushu, Japan
Correspondence: Professor I Akiba, Department of Chemistry and Biochemistry, The University of Kitakyushu, 1-1 Hibikino, Wakamatsu, Kitakyushu 8080135, Japan.
E-mail: akiba@kitakyu-u.ac.jp
Received 8 October 2015; revised 12 December 2015; accepted 24 January 2016; published online 16 March 2016

of hydrophobic molecules on their spatial distribution in polymer micelles.

EXPERIMENTAL PROCEDURE

Materials

We used BrBz and BrBzOH as models of Br-labeled hydrophobic molecules. Both chemicals were purchased from Wako Pure Chemicals Co. Ltd (Tokyo, Japan) and used as received.

The amphiphilic block copolymer P(*N*,*N*-dimethylaminoethyl methacrylate)-*block*-poly(methyl methacrylate) (PDMAEMA-*b*-PMMA) was synthesized via reversible addition–fragmentation radical polymerization.[26–28] A detailed description of the procedures used to synthesize and characterize the polymer, as well as the results, are provided in the Supplementary Information.

Table 1 shows the electron densities of each component in the block copolymer and hydrophobic molecule. Because the electron density of PDMAEMA was almost identical to that of water and much lower than that of PMMA, the scattering contribution of the PDMAEMA corona layer in small-angle X-ray scattering (SAXS) was ignored. Figure 1 shows the SAXS profile of PDMAEMA-*b*-PMMA micelles in aqueous solution. The experimental SAXS profile was in close agreement with the theoretical scattering curve calculated for a solid sphere with radius of 6 nm (solid line), although the estimated hydrodynamic radius of PDMAEMA-*b*-PMMA micelles according to dynamic light scattering was 11 nm. These results indicated that the scattering contribution of the corona in SAXS disappeared as a result of contrast matching between the corona and the solvent.

Preparation of PDMAEMA-*b*-PMMA micelles containing Br-labeled molecules

PDMAEMA-*b*-PMMA and BrBz or BrBzOH, which were soluble in PMMA, were combined to obtain a hydrophobic compound concentration of 10 wt% in PDMAEMA-*b*-PMMA. To produce micelles, the aforementioned mixture was dissolved in tetrahydrofuran and stirred at ambient temperature to produce a homogeneous solution. Subsequently, compared with the aforementioned solution, a fourfold excess of Millipore water (Merck Millipore, Darmstadt, Germany) was gradually added at a rate of 0.1 ml min^{-1} via a syringe pump. The resulting mixture was transferred to a dialysis tube (10 kDa molecular-weight cutoff) and dialyzed in a large volume of Millipore water for 1 week to remove tetrahydrofuran. During this procedure, precipitation did not occur. Finally, Millipore water was added to the micelle solution to obtain a micelle concentration of 1.0 mg ml^{-1}. PDMAEMA-*b*-PMMA micelles containing BrBz and BrBzOH were denoted as M(BrBz) and M(BrBzOH), respectively.

SAXS measurements

SAXS measurements were performed at BL-40B2 of SPring-8, Hyogo, Japan. A 30 cm × 30 cm imaging plate (Rigaku, Tokyo, Japan, R-AXIS VII) was placed at a distance of 2.0 m from the sample to cover a q range of 0.09 to 2.0 nm^{-1}. A bespoke vacuum sample chamber was used to reduce the scattering contribution of the background.[12] The X-ray transmittance of each sample was measured using an ion chamber located in front of the sample and a Si photodiode placed behind the sample. The measurements were carried out at five different incident X-ray energies: 12.40 keV (0.1 nm), 13.383 keV (0.927 nm), 13.433 keV (0.923 nm), 13.463 keV (0.921 nm) and 13.473 keV (0.920 nm). Except for 12.40 keV, the incident X-ray energies were close to the Br K-edge (13.483 keV). The sample solutions were packed in individual quartz capillaries with a light path length of 2.0 mm (Hilgenberg GmbH, Malsfeld, Germany) that were placed in the vacuum chamber. The exposure time of each SAXS measurement was limited to 60 s to avoid radiation damage, and five SAXS data measured for a sample at the same energy were integrated to improve the signal-to-noise ratio. Using circular averaging, the two-dimensional SAXS images were converted into profiles showing the intensity as a function of the magnitude of scattering vector q. Here, $q = (4\pi/\lambda)\sin(\theta/2)$, where θ is the scattering angle and λ is the wavelength of the incident X-ray. To obtain the excess scattering intensity, $I(q)$, at each vector, q, scattering from the solvent and the cell were subtracted after the appropriate correction for transmittance was applied. $I(q)$ was corrected to the absolute scale using the absolute scattering intensity of water (1.632×10^{-2} cm^{-1}). As shown below, $I(q)$ can only be compared using the same value of q in the ASAXS analysis, although changes in the energy of the incident X-ray lead to a shift in the q value assigned to a given pixel in the detector. Next, the SAXS profiles were interpolated using the cubic-spline method, without any smoothing or corrections to account for the q shift.[22–24]

Table 1 Electron densities (ρ) of components

	H_2O	PMMA	PDMAEMA	BrBz	BrBzOH
ρ/e^- nm^{-3}	333	380	334	434	456

Abbreviations: BrBz, bromobenzene; BrBzOH, 4-bromobenzylalcohol; PDMAEMA, poly(*N*,*N*-dimethylaminoethyl methacrylate); PMMA, poly(methyl methacrylate).

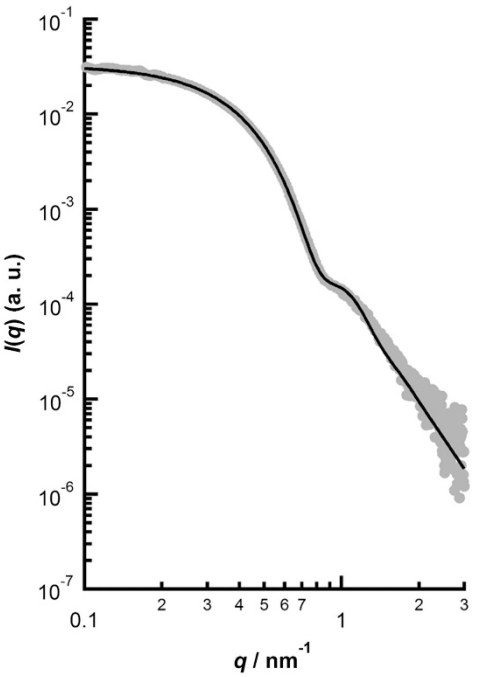

Figure 1 Small-angle X-ray scattering (SAXS) profile of poly(*N*,*N*-dimethylaminoethyl methacrylate)-*block*-poly(methyl methacrylate) (PDMAEMA-*b*-PMMA) micelles in aqueous solution. The gray circles represent experimental SAXS data. The solid line is the theoretical SAXS curve calculated for a solid sphere (R = 6.0 nm).

ASAXS analysis

The theoretical background of ASAXS has been described in detail elsewhere.[13,29] The SAXS intensity, $I(q)$, of homogeneously dispersed particles can be described as follows:

$$I(q) = NP(q)S(q) \quad (1)$$

where N is the number of particles per unit volume, $P(q)$ is the form factor and $S(q)$ is the structure factor defined from spatial correlations between the particles' center of mass. In dilute solutions, $S(q)$ can be assumed to be equal to 1. When the particles contain Br atoms and SAXS measurements are performed at the energy (E) of the incident X-ray near the Br K-edge, the atomic scattering factor $f(E)$ indicates the energy dependence because of the anomalous dispersion of Br.[29]

$$f(E) = f_0 + f'_{Br}(E) + if''_{Br}(E) \quad (2)$$

where f_0 is the normal atomic scattering factor and $f'_{Br}(E)$ and $f''_{Br}(E)$ are the real and imaginary components of the anomalous dispersion of Br, respectively.

In this case, the form factor represents the energy dependence, in accordance with the following formula:[13]

$$P(q,E) = P_0(q) + 2f'_{\mathrm{Br}}(E)F_0(q)V(q) + \left[f'_{\mathrm{Br}}(E) + if''_{\mathrm{Br}}(E)\right]V^2(q) \quad (3)$$

where $P(q, E)$ is the energy-dependent form factor of the particle, $P_0(q)$ is the nonresonant form factor of the particle obtained by normal SAXS measurement and $V(q)$ is the scattering amplitude of the spatial distribution of Br atoms. Consequently, $V^2(q)$ corresponds to the form factor of the spatial distribution of Br atoms. Figure 2 shows the energy dependence of $f'_{\mathrm{Br}}(E)$ and $f''_{\mathrm{Br}}(E)$. The closed circles represent f'_{Br} and f''_{Br} at the energies used in the present study, and the solid lines represent the effective $f'_{\mathrm{Br}}(E)$ and $f''_{\mathrm{Br}}(E)$ obtained from the convolution of theoretical $f'_{\mathrm{Br}}(E)$ and $f''_{\mathrm{Br}}(E)$ values[22,30] and the energy spread of the primary X-ray beam at the BL-40B2 station of SPring-8 ($\Delta E/E = 1\times10^{-4}$). $V^2(q)$ was obtained by solving the simultaneous equations of $P(q, E)$ that were measured using at least three different incident X-ray energies near the Br K-edge, in accordance with the following formula:[16,17]

$$V^2(q) = \frac{1}{K}\left[\frac{\Delta I(q,E_1,E_2)}{f'_{Br}(q,E_1) - f'_{Br}(q,E_2)} - \frac{\Delta I(q,E_1,E_3)}{f'_{Br}(q,E_1) - f'_{Br}(q,E_3)}\right] \quad (4)$$

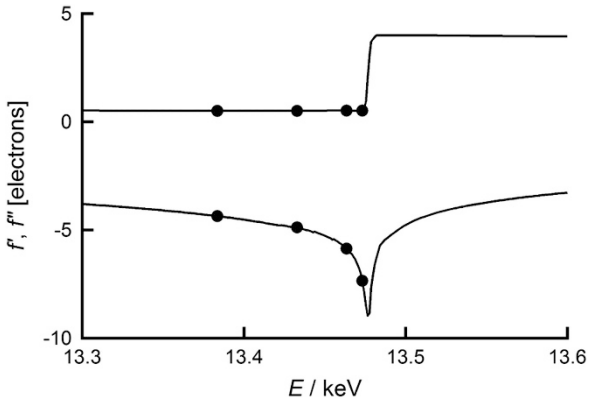

Figure 2 Energy dependence of the real and imaginary components of anomalous Br dispersion (f' and f''). The Br K-edge was 13.483 keV.

where

$$\Delta I(q, E_i, E_j) = 2\left[f'_{\mathrm{Br}}(E_i) - f'_{\mathrm{Br}}(E_j)\right]F_0(q)V(q) + \left[f''^{\,2}_{\mathrm{Br}}(E_i) + f''^{\,2}_{\mathrm{Br}}(E_j) - f'^{\,2}_{\mathrm{Br}}(E_i) - f'^{\,2}_{\mathrm{Br}}(E_j)\right]V^2(q) \quad (5)$$

$$K = f'_{Br}(E_2) - f'_{Br}(E_3) + \frac{f''^{\,2}_{Br}(E_1) - f''^{\,2}_{Br}(E_2)}{f'_{Br}(E_1) - f'_{Br}(E_2)} - \frac{f''^{\,2}_{Br}(E_1) - f''^{\,2}_{Br}(E_3)}{f'_{Br}(E_1) - f'_{Br}(E_3)} \quad (6)$$

Using $V^2(q)$ from the ASAXS analysis and $P_0(q)$ from the normal SAXS analysis, which was performed at an incident X-ray energy of 12.40 keV (0.1 nm), fitting analyses were conducted by applying theoretical scattering functions of suitable model particles.

RESULTS AND DISCUSSION

Figures 3a and b show the energy dependence of SAXS profiles for M(BrBz) and M(BrBzOH), respectively, measured at incident X-ray energies near the Br K-edge (13.483 keV). The SAXS intensities of these systems decreased when the energy of the incident X-ray approached from lower energies to the Br K-edge. As shown in Figure 2, $f'_{\mathrm{Br}}(E)$ decreased with an increase in the energy from the Br K-edge, whereas $f''_{\mathrm{Br}}(E)$ remained nearly constant. Therefore, the energy dependence of the SAXS intensities of M(BrBz) and M (BrBzOH) originated from the $f'_{\mathrm{Br}}(E)$s of BrBz and BrBzOH incorporated in PDMAEMA-*b*-PMMA micelles. The energy dependence of the SAXS intensities of M(BrBz) appeared in the high q region, whereas that of M(BrBzOH) was homogeneously distributed throughout the entire q range. According to Equation (3), differences in the energy-dependent SAXS profiles were attributable to differences in $V^2(q)$s that corresponded to the scattering amplitude of the spatial distribution of Br atoms. Therefore, this result suggests that the spatial distribution of hydrophobic molecules incorporated in polymer micelles was dependent on the presence or absence of hydroxyl groups. Thus, $V^2(q)$ profiles were extracted from the SAXS profiles by solving simultaneous equations

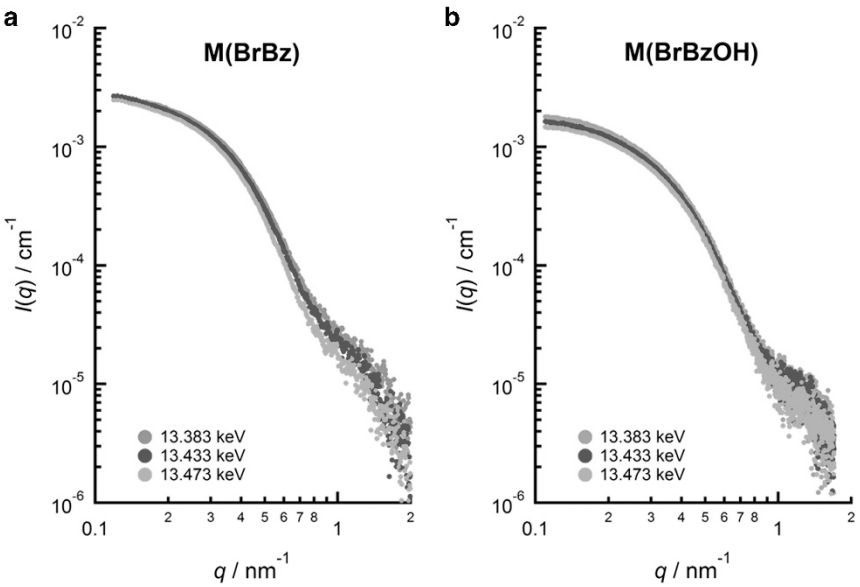

Figure 3 Energy dependence of the small-angle X-ray scattering (SAXS) profiles of (**a**) M(BrBz) and (**b**) M(BrBzOH) near the Br K-edge. M(BrBz), poly(*N*,*N*-dimethylaminoethyl methacrylate)-*block*-poly(methyl methacrylate) (PDMAEMA-*b*-PMMA) micelles containing bromobenzene; M(BrBzOH), PDMAEMA-*b*-PMMA micelles containing 4-bromobenzylalcohol. A full color version of this figure is available at *Polymer Journal* online.

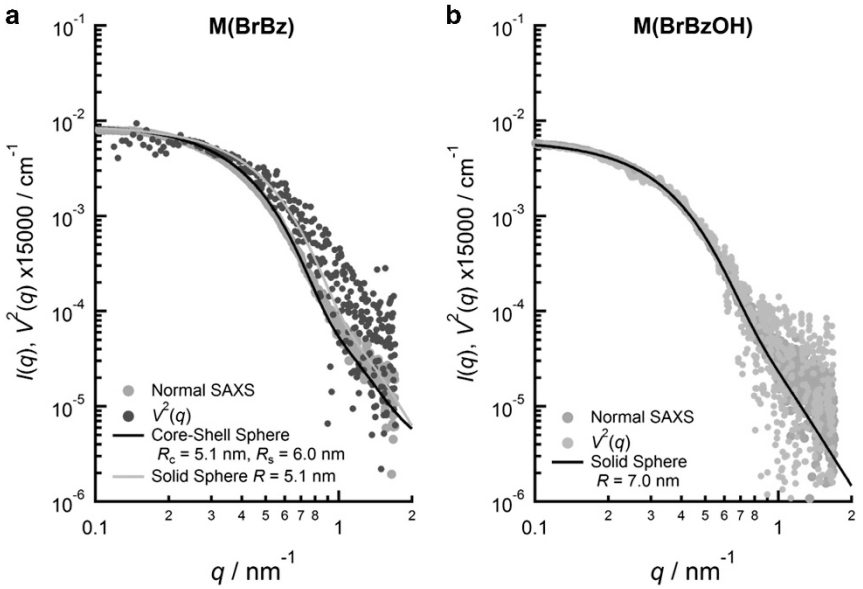

Figure 4 Comparison of normal small-angle X-ray scattering (SAXS) and $V^2(q)$ profiles of (**a**) M(BrBz) and (**b**) M(BrBzOH). M(BrBz), poly(*N*,*N*-dimethylaminoethyl methacrylate)-*block*-poly(methyl methacrylate) (PDMAEMA-*b*-PMMA) micelles containing bromobenzene; M(BrBzOH), PDMAEMA-*b*-PMMA micelles containing 4-bromobenzylalcohol. A full color version of this figure is available at *Polymer Journal* online.

of SAXS profiles measured at three different energies to determine the spatial distribution of Br-labeled hydrophobic molecules in PDMAEMA-*b*-PMMA micelles.

Figures 4a and b show the comparison between normal SAXS profiles that correspond to $P_0(q)$ in Equation (3) and were measured at 12.40 keV (0.1 nm) of incident X-ray energy, and the resulting $V^2(q)$ profiles of M(BrBz) and M(BrBzOH), respectively. As mentioned above, the normal SAXS profiles were considered the form factors of hydrophobic cores containing Br-labeled hydrophobic molecules, and the $V^2(q)$ profiles corresponded to the form factors of the spatial distribution of Br-labeled molecules. The $V^2(q)$ profile of M(BrBz) obviously deviated from the normal SAXS profile, whereas the $V^2(q)$ profile of M(BrBzOH) could be superimposed on the normal SAXS profile. Figure 5 shows the Guinier plots of normal SAXS and $V^2(q)$ profiles, and the resulting radii of gyration (R_g) for these two systems. R_g for the $V^2(q)$ profiles of M(BrBz) (4.0 nm) was slightly smaller than that of the normal SAXS profile (4.5 nm). However, for M(BrBzOH), R_g obtained from $V^2(q)$ was identical to that obtained from the SAXS profile (5.8 nm). These results suggested that BrBzOH was homogeneously dispersed in the hydrophobic PMMA core, whereas BrBz was segregated in a domain within the PMMA core. Thus, we examined the numerical analyses for the normal SAXS profiles and $V^2(q)$ profiles to clarify radial distributions of components in the hydrophobic core.

The solid lines in Figure 4 represent the theoretical SAXS curves calculated for the spherical particles provided below, and Table 2 summarizes the adjustable parameters used in the fitting analyses. Table 2 also lists the values of R_g/R, where R_g and R are the radius of gyration and particle radius, respectively. Generally, for a spherical particle, $R_g/R = 0.775$. Because the R_g/R values obtained from the analyses were close to 0.775, we concluded that spherical models could be used for the fitting analyses. For the $V^2(q)$ profiles, the fitting analyses were performed using the given spherical models, as shown in

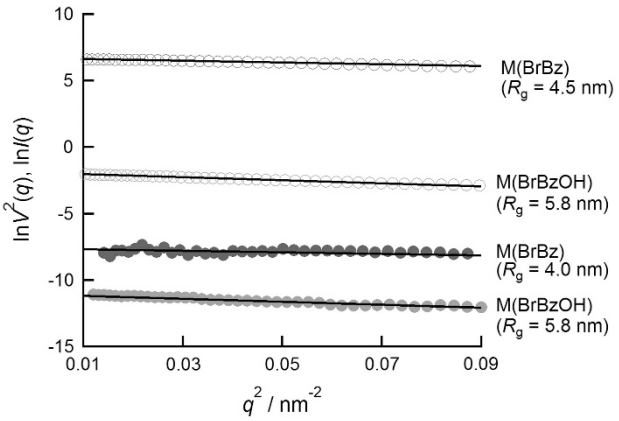

Figure 5 Guinier plots for normal small-angle X-ray scattering (SAXS) ($I(q)$) and resonant terms ($V^2(q)$) of M(BrBz) and M(BrBzOH). Open and filled circles represent $I(q)$ and $V^2(q)$, respectively. M(BrBz), poly(*N*,*N*-dimethylaminoethyl methacrylate)-*block*-poly(methyl methacrylate) (PDMAEMA-*b*-PMMA) micelles containing bromobenzene; M(BrBzOH), PDMAEMA-*b*-PMMA micelles containing 4-bromobenzylalcohol. A full color version of this figure is available at *Polymer Journal* online.

Equation (7).

$$P(q) = 9\left[\frac{\sin(qR) - qR\cos(qR)}{(qR)^3}\right]^2 \quad (7)$$

where R is the radius of a sphere. The results of the analyses are shown in Figure 4, with the red solid line indicating M(BrBz) and the solid line M(BrBzOH). For M(BrBzOH), the normal SAXS profile was also in agreement with the sphere model with a radius of 7.0 nm. Consequently, BrBzOH molecules were homogeneously dispersed in the PMMA core of the PDMAEMA-*b*-PMMA micelles. In contrast, the normal SAXS profile of M(BrBz) did not agree with the fitted results for the $V^2(q)$ profile. Thus, we analyzed the SAXS profile of

Table 2 Parameters from the numerical analyses with the model particles

Profile	*Model*	R_h/*nm*	R_C/*nm*	$\rho_h/e^-/nm^3$	$\rho_C/e^-/nm^3$	$\rho_O/e^-/nm^3$	Z[a]	R_g/*nm*[b]	R_g/R[c]
M(BrBz)									
$V^2(q)$	Sphere	5.1	—	—	—	—	25	4.0	0.78
$I(q)$	Core–shell sphere	5.1	6.0	391	377	333	30	4.5	0.75
M(BrBzOH)									
$V^2(q)$	Solid sphere	7.0	—	—	—	—	30	5.8	0.83
$I(q)$	Solid sphere	7.0	7.0	387	—	333	30	5.8	0.83

Abbreviations: M(BrBz), poly(*N,N*-dimethylaminoethyl methacrylate)-*block*-poly(methyl methacrylate) (PDMAEMA-*b*-PMMA) micelles containing bromobenzene; M(BrBzOH), PDMAEMA-*b*-PMMA micelles containing 4-bromobenzylalcohol.
[a]*Z* is a parameter of polydispersity in Schultz distribution function. *Z* is related to the s.d. σ by $\sigma=(Z+1)^{-1/2}$.
[b]R_gs were obtained from the Guinier plots for $V^2(q)$ or $I(q)$ shown in Figure 5.
[c]R_g/R corresponds to R_g/R_h for $V^2(q)$ and R_g/R_C for $I(q)$.

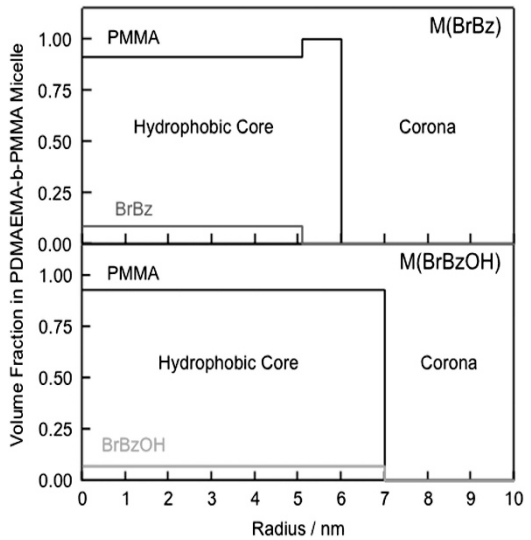

Figure 6 Radial distribution of the volume fraction of components in M(BrBz) and M(BrBzOH) obtained via normal small-angle X-ray scattering (SAXS) and anomalous SAXS (ASAXS) analyses. M(BrBz), poly(*N,N*-dimethylaminoethyl methacrylate)-*block*-poly(methyl methacrylate) (PDMAEMA-*b*-PMMA) micelles containing bromobenzene; M(BrBzOH), PDMAEMA-*b*-PMMA micelles containing 4-bromobenzylalcohol. A full color version of this figure is available at *Polymer Journal* online.

M(BrBz) using a core–shell sphere model given by the following equation:[31]

$$I(q) = N\left\{(\rho_h-\rho_C)V_h\frac{3[\sin(qR_h)-qR_h\cos(qR_h))}{(qR_h)^3} + (\rho_C-\rho_0)V_C\frac{3[\sin(qR_C)-qR_C\cos(qR_C))}{(qR_C)^3}\right\}^2 \quad (8)$$

where V_C is the volume of the hydrophobic core, V_h is the volume of the BrBz-segregated region within the hydrophobic core, R_h and R_C are the radii of the BrBz-segregated domain and the hydrophobic core, respectively, and ρ_h, ρ_C and ρ_0 are the electron densities of the BrBz-segregated domain, hydrophobic core and background, respectively. Here, R_h was set to 5.1 nm, as estimated by the fitting analysis for $V^2(q)$ of M(BrBz). The solid line in the normal SAXS profile of M(BrBz) in Figure 4a shows the fitting result, and Figure 6 shows the radial distribution of hydrophobic components in the hydrophobic core for M(BrBz) and M(BrBzOH) that was estimated from the radial electron density profiles obtained using the fitting analyses shown in Table 2. In M(BrBz), a depletion layer of BrBz molecules existed in the vicinity of the core–corona interface. Previous studies have reported that PMMA was swollen with water at the interface;[32] therefore, the depletion layer of BrBz molecules should be formed to avoid contact with water penetrating the PMMA core. In contrast, BrBzOH was homogeneously dispersed in the hydrophobic PMMA core. The affinity of BrBzOH molecules for water should be higher than that of BrBz because of the presence of its hydroxyl group. Consequently, BrBzOH can homogeneously disperse in the hydrophobic PMMA core, even in the vicinity of the core–corona interface. Thus, the difference in the spatial distributions of BrBz and BrBzOH in the PMMA core was because of the difference in hydrophobicity between BrBz and BrBzOH. The results of the present study indicate that hydrophobicity enhances segregation of hydrophobic molecules in the core. Therefore, drug molecules with strong hydrophobicity should be stably retained in polymer micelles owing to firm encapsulation in the hydrophobic core. In our future work, we will examine the relationship between the retention and spatial distribution of hydrophobic molecules in the hydrophobic cores of polymer micelles.

CONCLUSION

The spatial distribution of BrBz and BrBzOH incorporated into the hydrophobic PMMA core of PDMAEMA-*b*-PMMA micelles was investigated using ASAXS near the Br K-edge. The region containing BrBz molecules was slightly smaller than the hydrophobic core. As a result, a depletion layer of BrBz formed in the vicinity of the core–corona interface because of segregation of BrBz molecules from water penetrating the PMMA core. In contrast, BrBzOH molecules were homogeneously dispersed in the PMMA core. Because the presence of a hydroxyl group in BrBzOH enhanced its affinity to water present in the PMMA core, BrBz molecules existed in the vicinity of the core–corona interface. The results of this work suggest that the spatial distribution of polymer micelles can be tuned by controlling the hydrophobicity or polarity of hydrophobic molecules.

CONFLICT OF INTEREST

The authors declare no conflict of interest.

ACKNOWLEDGEMENTS

Generous financial support was provided by MEXT, Japan (Photon and Quantum Basic Research Coordinated Development Program). SAXS measurements were performed under the approval of the SPring-8 Advisory Committee (2012B1528, 2013B1277 and 2014B1419 for IA, 2013B1683 for MK and 2015A1331 for RN).

1 Zhang, L. F. & Eisenberg, A. Multiple morphologies of "crew-cut" aggregates of polysyrene-*b*-poly(acrylic acid) block copolymers. *Science* **268**, 1728–1731 (1995).
2 Yokoyama, M. in *Polymeric Drug Delivery Systems* (ed. Kwon G. S.) 533–575 (Taylor & Francis, Boca Raton, FL, USA, 2005).
3 Yokoyama, M., Okano, T., Sakurai, Y., Fukushima, S., Okamoto, K. & Kataoka, K. Selective delivery of adiramycin to a solid tumor using a polymeric micelle carrier system. *J. Drug Targeting* **7**, 171–186 (1999).
4 Monfardini, C. & Veronese, F. M. Stabilization of substances in circulation. *Bioconjugate Chem.* **9**, 418–450 (1998).
5 Matsumura, Y., Kimura, M., Yamamoto, T. & Maeda, H. Involvement of the kinin-generating cascade in enhanced vascular permeability in tumor tissue. *Jpn J. Cancer Res.* **79**, 1327–1334 (1988).
6 Maeda, H. SMANCS and polymer-conjugated macromolecular drugs: advantages in cancer chemotherapy. *Adv. Drug Delivery Rev.* **6**, 181–202 (1991).
7 Nakanishi, T., Fukushima, S., Okamoto, K., Suzuki, M., Matsumura, Y., Yokoyama, M., Okano, T., Sakurai, Y. & Kataoka, K. Development of the polymer micelle carrier system for doxorubicin. *J. Control. Release* **74**, 295–302 (2001).
8 Fang, J., Nakamura, H. & Maeda, H. The EPR effect: unique features of tumor blood vessels for drug delivery, factors involved, and limitations and augmentation of the effect. *Adv. Drug Delivery Rev.* **63**, 136–151 (2011).
9 Yamamoto, T., Yokoyama, M., Opanasopit, P., Hayama, A., Kawano, K. & Maitani, Y. What are determining factors for stable drug incorporation into polymeric micelle carriers? Consideration on physical and chemical characters of the micelle inner core. *J. Control. Release* **123**, 11–18 (2007).
10 Yokoyama, M., Opanasopit, P., Okano, T., Kawano, K. & Maitani, Y. Polymer design and incorporation methods for polymeric micelle carrier system containing water-insoluble anti-cancer agent camptothecin. *J. Drug Target.* **12**, 373–384 (2004).
11 Satoh, T., Higuchi, Y., Kawakami, S., Hashida, M., Kagechika, H., Shudo, K. & Yokoyama, M. Encapsulation of the synthetic retinoids Am80 and LE540 into polymeric micelles and the retinoids' release control. *J. Control. Release* **136**, 187–195 (2009).
12 Akiba, I., Terada, N., Hashida, S., Sakurai, K., Sato, T., Shiraishi, K. & Yokoyama, M. Encapsulation of a hydrophobic drug into a polymer-micelle core explored with synchrotron SAXS. *Langmuir* **26**, 7544–7551 (2010).
13 Stuhrmann, H. B. Resonant scattering in macromolecular structure research. *Adv. Polym. Sci.* **67**, 123–163 (1985).
14 Polizzi, S., Riello, P., Goerigk, G. & Benedetti, A. Quantitative investigations of supported metal catalysts by ASAXS. *J. Synchrotron Radiat.* **9**, 65–70 (2002).
15 Svergun, D. I., Kozin, M. B., Konarev, P. V., Shtykova, E. V., Volkov, V. V., Chernyshov, D. M., Valetsky, P. M. & Bronstein, L. M. Formation of metal nanoparticles in multilayered poly(octadecylsiloxane) as revealed by anomalous small-angle X-ray scattering. *Chem. Mater.* **12**, 3552–3560 (2000).
16 Goerigk, G., Schweins, R., Huber, K. & Ballauff, M. The distribution of Sr^{2+} counterions around polyacrylate chains analyzed by anomalous small-angle X-ray scattering. *Europhys. Lett.* **66**, 331–337 (2004).
17 Patel, M., Rosenfeldt, S., Ballauff, M., Dingenouts, N., Pontoni, D. & Narayanan, T. Analysis of the correlation of counterions to rod-like macroions by anomalous small-angle X-ray scattering. *Phys. Chem. Chem. Phys.* **6**, 2962–2967 (2004).
18 Dingenouts, N., Patel, M., Rosenfeldt, S., Pontoni, D., Narayanan, T. & Ballauff, M. Counterion distribution around a spherical polyelectrolyte brush probed by anomalous small-angle X-ray scattering. *Macromolecules* **37**, 8152–8159 (2004).
19 Goerigk, G., Huber, K. & Schweins, R. Probing the extent of the Sr^{2+} ion condensation to anionic polyacrylate coils: a quantitative anomalous small-angle X-ray scattering study. *J. Chem. Phys.* **127**, 154908 (2007).
20 Varga, Z., Berényi, S., Szokol, B., Őrfi, L., Kéri, G., Peták, I., Hoell, A. & Bóta, A. A closer look at the structure of sterically stabilized liposomes: a small-angle X-ray scattering study. *J. Phys. Chem. B* **114**, 6850–6854 (2010).
21 Sztucki, M., Cola, E. D. & Narayanan, T. New opportunities for anomalous small-angle X-ray scattering to characterize charged soft matters systems. *J. Phys. Conf. Ser.* **272**, 012004 (2011).
22 Akiba, I., Takechi, A., Sakuo, M., Handa, M., Shinohara, Y., Amemiya, Y., Yagi, N. & Sakurai, K. Anomalous small-angle X-ray scattering study of structure of polymer micelles having bromines in hydrophobic core. *Macromolecules* **45**, 6150–6157 (2012).
23 Sakou, M., Takechi, A., Handa, M., Shinohara, Y., Amemiya, Y., Masunaga, H., Ogawa, H., Yagi, N., Sakurai, K. & Akiba, I. Anomalous small-angle X-ray scattering study on aggregation of a block copolymer in a selective solvent. *J. Phys. Conf. Ser.* **272**, 012022 (2011).
24 Sakou, M., Takechi, A., Murakami, S., Sakurai, K. & Akiba, I. Study on the internal structure of polymer micelles by anomalous small-angle X-ray scattering at two edges. *J. Appl. Cryst.* **46**, 1407–1413 (2013).
25 Sanada, Y., Akiba, I., Sakurai, K., Shiraishi, K., Yokoyama, M., Mylonas, E., Ohta, N., Yagi, N., Shinohara, Y. & Amemiya, Y. Hydrophobic molecules infiltrating into the poly (ethylene glycol) domain of the core/shell interface of a polymeric micelle: evidence obtained with anomalous small-angle X-ray scattering. *J. Am. Chem. Soc.* **135**, 2574–2582 (2013).
26 Chiefari, J., Chong, Y. K., Ercole, F., Kristina, J., Jeffery, J., Le, T. P. T., Mayadunne, R. T. A., Meijs, G. F., Moad, C. L., Moad, G., Rizzardo, E. & Thang, S. H. Living free-radical polymerization by reversible addition-fragmentation chain transfer. The RAFT process. *Macromolecules* **31**, 5559–5562 (1998).
27 Yali, L., Akiba, I., Harrisson, S. & Wooley, K. L. Facile formation of uniform shell-crosslinked nanoparticles with built-in functionalities from N-hydroxysuccinimide-activated amphiphilic block copolymers. *Adv. Funct. Mater.* **18**, 551–559 (2008).
28 Yali, L., Du, W., Sun, G. & Wooley, K. L. pH-responsive shell cross-linked nanoparticles with hydrolytically labile cross-links. *Macromolecules* **41**, 6605–6607 (2008).
29 Lund, R., Willner, L., Lindner, P. & Richter, D. Structural properties of weakly segregated PS-PB block copolymer micelles in n-alkanes: solvent entropy effects. *Macromolecules* **42**, 2686–2695 (2009).
30 Sasaki, S. Anomalous scattering factors for synchrotron radiation users, calculated using Cromer and Liberman's method. *KEK Rep.* 88–14 (1989).
31 Nakano, M., Deguchi, M., Matsumoto, K., Matsuoka, H. & Yamaoka, H. Self-assembly of poly(1,1-diethylsilabutane)-*block*-poly(2-hydroxuethyl methacrylate) block copolymer. 1. Micelle formation and micelle-unimer-reversed micelle transition by solvent composition. *Macromolecules* **32**, 7437–7443 (1999).
32 Tanaka, K., Fujii, Y., Atarashi, H., Akabori, K., Hino, M. & Nagamura, T. Nonsolvents cause swelling at the interface with poly(methyl methacrylate) films. *Langmuir* **24**, 296–301 (2008).

Supplementary Information accompanies the paper on Polymer Journal website (http://www.nature.com/pj)